ELSEVIER

Processing metallic glasses by selective laser melting

Simon Pauly[1], Lukas Löber[1,2,*], Romy Petters[1,*], Mihai Stoica[1], Sergio Scudino[1], Uta Kühn[1] and Jürgen Eckert[1,2]

[1] IFW Dresden, Institut für Komplexe Materialien, Helmholtzstraße 20, D-01069 Dresden, Germany
[2] TU Dresden, Institut für Werkstoffwissenschaft, D-01062 Dresden, Germany

Metallic glasses and their descendants, the so-called bulk metallic glasses (BMGs), can be regarded as frozen liquids with a high resistance to crystallization. The lack of a conventional structure turns them into a material exhibiting near-theoretical strength, low Young's modulus and large elasticity. These unique mechanical properties can be only obtained when the metallic melts are rapidly cooled to bypass the nucleation and growth of crystals. Most of the commonly known and used processing routes, such as casting, melt spinning or gas atomization, have intrinsic limitations regarding the complexity and dimensions of the geometries. Here, it is shown that selective laser melting (SLM), which is usually used to process conventional metallic alloys and polymers, can be applied to implement complex geometries and components from an Fe-base metallic glass. This approach is in principle viable for a large variety of metallic alloys and paves the way for the novel synthesis of materials and the development of parts with advanced functional and structural properties without limitations in size and intricacy.

Introduction

In past decades metallic glasses, or synonymously amorphous metallic alloys, have transformed from a lab curiosity into a thoroughly and intensely investigated matter within the fields of physics and materials science [1–3]. In the early days of metallic glass research, glasses could be only prepared under extremely high cooling rates, which only allowed the synthesis of samples in the shape of thin ribbons or splat-quenched droplets [2–6]. Subsequent advances in the understanding of vitrification and technological advances in terms of processing have led to the development of metallic glasses with a wider range of geometries, even on the order of centimeters, termed bulk metallic glasses (BMGs) [2,6,7]. Today, a huge variety of glass-forming alloys is known, most of which consist of at least three elements; generally, metals, late and early transition metals and metalloids [2,3,6].

*Corresponding authors:. Löber, L. (l.loeber@ifw-dresden.de), Petters, R. (r.petters@ifw-dresden.de)

Glass formation in metallic alloys

When a metallic melt is cooled under equilibrium conditions it adopts the state of lowest energy, which means it crystallizes after a certain degree of undercooling [8,9]. In a schematic continuous cooling transformation (CCT) diagram (Fig. 1) crystallization is indicated by the intersection of the cooling rate curve, R_{cryst}, with the crystalline 'nose'.

In order to prevent a metallic melt from crystallizing, but to vitrify instead, the melt has to be cooled faster, viz. at rates exceeding the critical value, R_c (Fig. 1). At the same time, the alloy system must obey several constraints: the alloy should have a low driving force for crystallization [10] and/or structural relaxation should be slowed down in order to hamper atomic rearrangements upon cooling [2,6,8]. While the driving force of crystallization is a thermodynamic property, structural relaxation represents the system's kinetics and reflects macroscopically in the viscosity of the supercooled melt [9,10]. Both thermodynamic and kinetic parameters affect the melt's resistance against crystallization and shift the crystalline phase field in the CCT diagram to larger times [11]. This, in turn, means that the intrinsic critical cooling rate decreases and

1369-7021/06 http://dx.doi.org/10.1016/j.mattod.2013.01.018

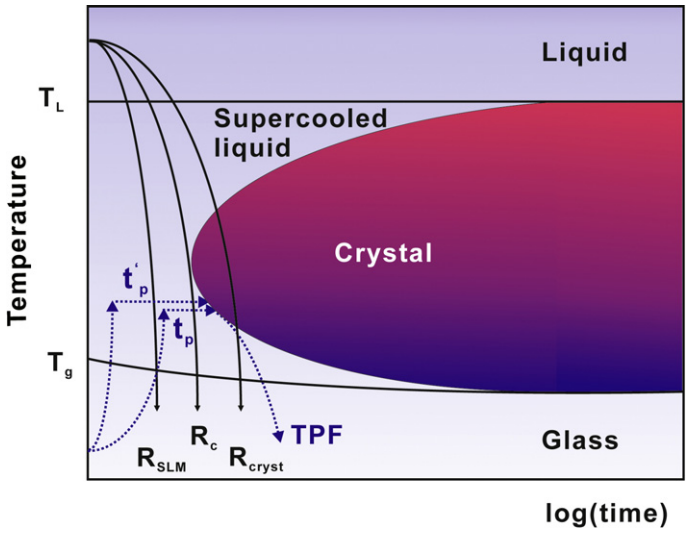

FIGURE 1

Schematic CCT diagram for a metallic glass former. Vitrification occurs when the melt is cooled at rates higher than the critical cooling rate, R_c. At lower cooling rates, R_{cryst} for example, the crystalline 'nose' is crossed and the melt partially or fully crystallizes. This is generally avoided during SLM as it has high intrinsic cooling rates, R_{SLM}. In the course of thermoplastic forming (TPF) the glass is heated into its supercooled liquid region and brought into the desired shape in a maximum time, t_p. Subsequently, the supercooled liquid has to be cooled to room temperature at sufficiently high rates. When the heating step is finished in an extremely short time [30] the processing window increases to t'_p.

consequently the glass-forming ability of the system, that is, its tendency to vitrify, improves (cf. Fig. 1). Depending on the exact alloy composition and the preparation route, such as melt-spinning [12] or casting [2], typical critical cooling rates are on the order of 10^2–10^6 K/s [2,6,13,14].

In a nutshell, metallic glasses can be obtained when the liquid state is extraordinarily stable and the heat of the melt is extracted rapidly. Under these conditions the structure of the liquid can be retained in the solid state. Hence one of the most prominent characteristics of metallic glasses is the absence of conventional ordering: As opposed to the crystalline lattice with its translational symmetry, metallic glasses lack any long-range order and only show a weak ordering on the short- and medium-range scales [3,15–17]. This disordered atomic arrangement determines the unusual structural and functional properties of (bulk) metallic glasses, which have been summarized in comprehensive reviews [1–3,6,18,19]. Yet, to name but a few features, BMGs deform plastically via highly localized shear bands, which directly results in high yield stresses of up to 5 GPa [20] and makes amorphous alloys materials with near-theoretical strength [21,22]. Furthermore, their Young's moduli are lower than those of the corresponding crystalline state materials, which consequently results in a large elastic strain of about 2% [19,23]. This unconventional behavior to mechanical loading makes bulk metallic glasses interesting candidates for structural applications such as springs, hinges, gears and micro-electro-mechanical systems (MEMS), amongst others [3,13,18]. Fe-based metallic glasses and related compositions also stand out because of their unmatched soft-magnetic behavior with a low coercivity and low remanence, as is optimal for the cores of high-frequency transformers or magnetic shielding components in microelectronics [24].

However, the full potential of amorphous alloys has not yet been exploited, because of technological limitations: the requirement to rapidly extract the heat from the melt imposes severe restrictions on the fabrication methods [8,11]. The most commonly applied process is casting, but other processing routes can be used to prepare amorphous alloys [4,9,21]. For casting, it is essential that the molds, in which the melt solidifies, consist of a material with high thermal conductivity and large heat capacity like Cu. When the mold cavity is large and thus the cooling rate is low, the glass-forming ability of the given system has to be high for the production of a metallic glass [6,11]. The intrinsic trade-off of casting is that either good glass formers are required or the size of the parts is rather limited (below about 1 mm) [11]. Moreover, only simple geometries – typically rods or plates – can be prepared [3,13,18]. When more complex shapes are required the capabilities of casting are insufficient and different processes have to be employed. One option is to heat the glass into its supercooled liquid region, the temperature regime between the glass transition temperature (T_g) and the crystallization temperature (T_x). Above T_g the viscosity of supercooled metallic liquids tends to decrease rapidly [8,25], which allows thermoplastic forming of the material, similar to the processes used for silicate glasses and polymers [26,27] (and references therein). The typical temperature profile for thermoplastic forming (TPF) is indicated in Fig. 1. Even though this process has specific advantages, such as a near-net-shape finish, extremely smooth surfaces and the ability to replicate even nanometer scale structures [26–28], the time window for processing (t_p) is generally quite limited. Shaping only works in the supercooled liquid region at relatively low viscosities and it has to be completed before crystallization interferes [26,27]. Considering the time needed to heat the glass into its supercooled liquid region and to quench it back into the glassy state, essentially only strong glass formers can be treated this way [26,27]. Unfortunately, these good glass formers or bulk metallic glasses often contain toxic (Be) or expensive elements (Pt, Pd, Au etc.) [7,13,29].

In order to increase the time for the actual shaping or forming process, the heating of the glass can be performed in milliseconds by quasi-adiabatic, ohmic heating, as has been demonstrated recently [30]. This approach is feasible due to the high electrical resistivity of amorphous alloys [13,21,30], which causes a significant heating when a current is passed through it. As shown in Fig. 1, the available time window for forming under these extreme conditions increases to t'_p. Still, a major drawback is that complex hollow and/or large-scale structures for instance are difficult if not impossible to be obtained through thermoplastic forming.

Therefore, there is a certain necessity to explore and develop novel processing routes for the synthesis of complicated amorphous components. According to the brief discussion above it is immediately plausible that a layer-additive manufacturing (LAM) process – such as selective laser melting (SLM) [31] – would be highly advantageous for the manufacturing of complex and large-scale parts. Because of the layer-wise construction of the part, the geometries obtainable are freestanding and do not rely on specific molds.

Selective laser melting (SLM)

The operating mode of selective laser melting (SLM) [31–33] is sketched in Fig. 2: a powder is placed on top of a base plate (Fig. 2a),

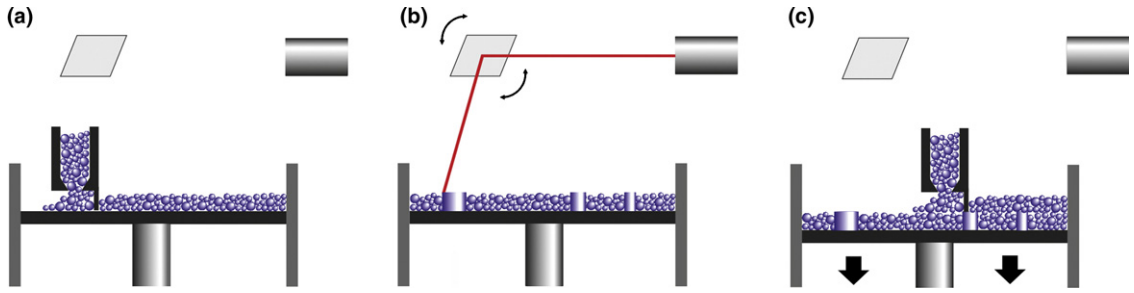

FIGURE 2

Illustration of the SLM operating mode: (a) a layer of powder is placed on the base plate. (b) Then a high-power laser melts the powder in spots previously defined by a 3D CAD model of the structure. The melt solidifies quickly and fuses with the structures below to form a solid piece. (c) Once the illumination process is finished the entire bas plate is lowered, the next powder layer is added and the process starts again at (a).

which is required as a support for the final part and which is detached from it after completion of the manufacturing process [31–33]. State-of-the art materials for the base plate generally are iron-, titanium-, aluminum- or nickel-base, which guarantee mechanical stability and good heat dissipation [31,32]. The powder is then melted locally after the illumination with a focused high-power laser (Fig. 2b). In the present work an ytterbium-fiber laser operating at a wavelength of 1070 nm and a maximum power of 400 W was applied. The melt immediately freezes and bonds to the bottom plate when the laser moves on. In the next step, a second powder layer is added and the laser again melts the material in defined spots leading to fusion of the melt and the subjacent material (Fig. 2c). To reduce unwanted contamination the entire process takes place under a protective atmosphere such as nitrogen, argon or helium [31,32].

Depending on the size of the laser spot, the laser power and the dwelling time, the energy input into the powder can be controlled and consequently so can the quantity of molten powder [34]. This allows the generation of a relatively small melt puddle (on the order of 100 μm) [35], which greatly facilitates the rapid heat extraction required for glass formation. Solidification thus occurs relatively quickly during SLM, especially when the thermal conductivity of the material underneath is high and generally reaches values on the order of 10^3–10^4 K/s [34]. The local intrinsic cooling rate, R_{SLM}, can thus be high enough to bypass the crystalline nose in the CCT diagram for glass-forming compositions (Fig. 1).

In the past, mainly conventional metals and alloys as well as polymers have been processed by SLM [31] and up to date it has not been investigated whether or not it is possible to fabricate glassy metallic components using glass-forming powders in the SLM process.

In the following, we describe the fabrication and characterization of a relatively complex three-dimensional scaffold structure by SLM consisting of a gas-atomized glass-forming Fe-based powder. The powder was obtained by electron-induction melting gas atomization (EIGA) of the according pre-alloy. Thereby, a jet of the molten alloy is finely dispersed in an Ar-stream and the resulting droplets are then collected [36]. Prior to processing the powder with a nominal composition of $Fe_{74}Mo_4P_{10}C_{7.5}B_{2.5}Si_2$ [37] (TLS Technik GmbH & Co. Spezialpulver KG) in a SLM 250 HL (SLM Solutions), it was dry-sieved under Ar and only those particles with a size $d_{90} < 50$ μm were selected. As the scanning electron micrograph (Fig. 3a) proves, the powder particle size extends from a few micrometers up to 50 μm and the particle surfaces are very smooth. The powder was de-magnetized through heat treatment above the Curie temperature (693 K) in order to increase its flowability and decrease its tendency to agglomerate, which is crucial for the SLM process. This particular Fe-based composition was chosen because of its relatively good glass-forming ability [37], its cheap constituent elements, which make it a realistic candidate for applications. Another advantage is the relatively low affinity towards oxygen, which makes it much easier to handle compared to Ti-base or Zr-base alloys.

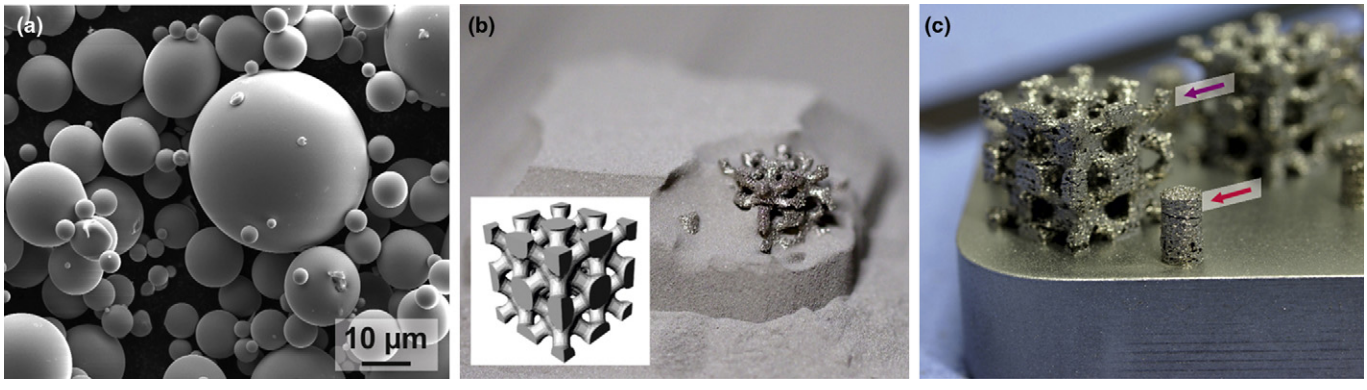

FIGURE 3

(a) Scanning electron microscopy image of the gas-atomized $Fe_{74}Mo_4P_{10}C_{7.5}B_{2.5}Si_2$ powder. (b) The inset depicts the 3D scaffold structure generated in a CAD program. The finished structure, which is still embedded in the powder, is visible. (c) The final scaffolds on top of the base plate (316L steel). The purple arrow indicates from where samples were taken for X-ray diffraction and DSC measurements. As reference also the cylinders next to the scaffolds (see red arrow) were characterized the same way.

In the very first step the SLM parameters had to be adapted to the material and had to be optimized to produce a mostly dense and defect-free component. Gradually, the laser power, the scanning speed, the distance between the laser tracks and the layer thickness were systematically varied until a feasible set of parameters was established (laser power: 320 W, scanning speed 3470 mm/s, distance between the laser tracks: 0.124 mm and layer thickness: 50 μm). Subsequently, the lattice structure displayed in the inset to Fig. 3b was generated by a CAD program and the processing of the $Fe_{74}Mo_4P_{10}C_{7.5}B_{2.5}Si_2$ powder was carried out. Fig. 3b shows the final component still being embedded in the powder bed, whereas the entire scaffold on top of the base plate is depicted in Fig. 3c. Due to the high cooling rate [34], the limited malleability of the Fe-based glass [37] and the still non-optimum processing parameters, small cracks and pores appear in the scaffold and the reference cylinder (Fig. 3c).

In Fig. 3c it is also marked from where material was removed to be characterized by X-ray diffraction (Philips PW1050 with Co-K_α radiation) and differential scanning calorimetry (DSC, Netzsch DSC 404 and Perkin-Elmer Diamond).

The results from X-ray diffraction of the powder, the reference cylinder, the corners of the scaffold as well as of a reference melt-spun ribbon are summarized in Fig. 4. The ribbon was prepared directly from the gas-atomized powder by single-roller melt spinning in order to evaluate the influence of different cooling rates.

The diffraction patterns of the powder, the SLM-cylinder and the SLM-component are nearly identical and are all characterized by sharp reflections being superimposed on a broad maximum around $2\theta = 51°$. As indexed in Fig. 4 the main reflections correspond to α-Fe, γ-Fe and $Fe_{23}B_6$. The Bragg peaks have low intensities and are relatively broad, which indicates that the grain size is in the sub-micron regime and that the crystalline volume fraction is not very high. Only the ribbon appears to be fully amorphous, showing only the broad diffraction maxima typical of disordered matter. This is somewhat astonishing as $Fe_{74}Mo_4P_{10}C_{7.5}B_{2.5}Si_2$ has been reported to vitrify into rods up to 5 mm in diameter [37] and consequently the gas-atomized powder should be also fully amorphous. Therefore, the exact chemical composition was determined by ICP-OES (inductively-coupled optical emission spectroscopy) and Cu (0.035 wt.%), Ni (0.230 wt.%) and Ti (0.460 wt.%) were detected as the main contaminants. This small change in the composition seems to be detrimental to the glass-forming ability of this system [37,38] and only the cooling rates of melt spinning, which are higher than for gas-atomization (10^2–10^4) [36,39,40], allow the melt to fully circumvent crystallization.

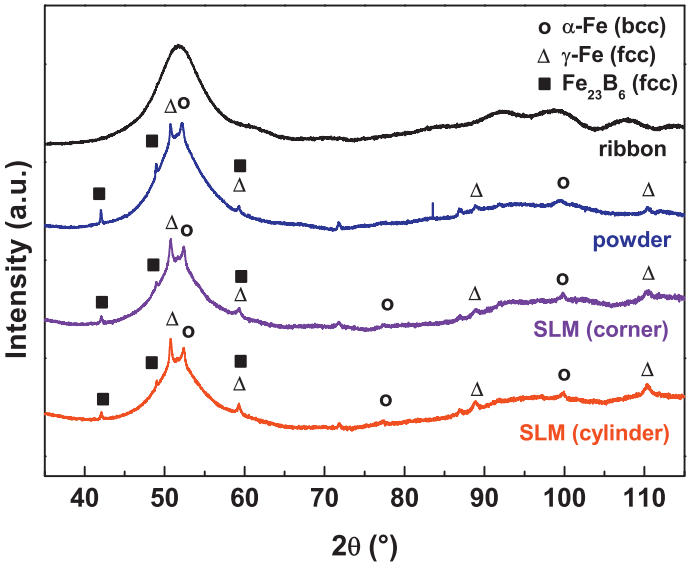

FIGURE 4

X-ray diffraction patterns (Co-K_α, $\lambda = 1.7903$ Å) of the ribbon produced from the gas-atomized powder, of the powder itself, of a corner of the scaffold and of the cylinder (see arrows in Fig. 3c). Only the ribbon exhibits the broad diffraction maxima typical of glasses. In the other cases crystalline (Bragg) reflections are superimposed pointing to a mixture of glass and nanocrystalline phases. Interestingly, also the gas-atomized powder appears to be partially crystalline, which is attributed to the presence of contaminants (Cu, Ni and Ti).

What is more important here is the fact that the diffraction patterns do not markedly differ prior to and after the SLM process. A significant change in the crystalline volume fraction or a substantial crystal growth can similarly not be measured that – in principle – could have been caused by the energy input of the laser. In other words, the structure of the material appears to be stable during SLM.

Subsequently, the thermal stability and crystallization behavior of the different samples was assessed by DSC measurements and the results are given in Fig. 5. All specimens exhibit a distinct glass transition followed by a multi-stage crystallization process (see arrow in inset to Fig. 5). The occurrence of the glass transition is definite proof that the scaffold contains an amorphous phase. It is beyond the scope of this publication to reveal the details of the crystallization mechanism.

To additionally analyze the effect of the SLM process on the structure of the gas-atomized powder, the enthalpies of crystallization were calculated for the different specimens and found to be 35 ± 2 J/g for the gas-atomized powder, 36 ± 2 J/g for the reference cylinder and 37 ± 2 J/g for the corner of the scaffold. The values are thus consistent within experimental error and

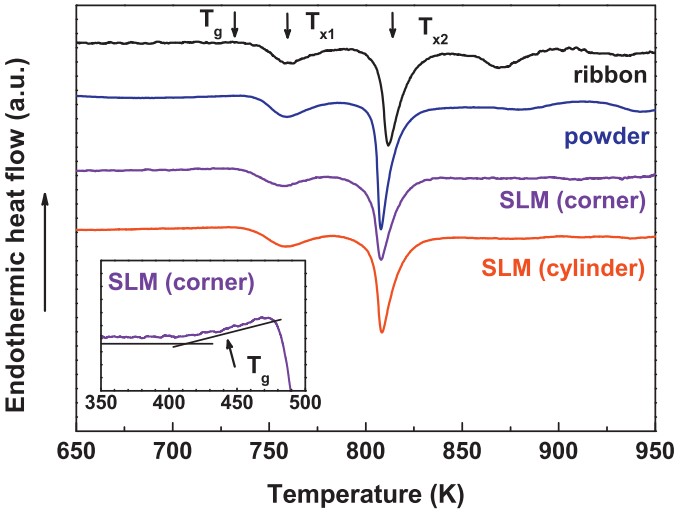

FIGURE 5

DSC traces recorded at a heating rate of 20 K/min. All samples crystallize in multiple steps marked by the arrows, T_{x1} and T_{x2} and the inset enlarges the glass transition regime as determined in the low-temperature DSC device at a heating rate of 40 K/min. The arrow marks the endothermic event connected to the glass transition.

corroborate the assumption from the X-ray diffraction experiments: The crystalline volume fraction does not increase after the melting and subsequent solidification during manufacturing. Hence, SLM is in principal capable to yield amorphous parts with complex shapes.

Conclusions and outlook

At present it is great challenge to produce large-scale glassy alloys in sophisticated geometries with the existing technologies. This is because of the metastable nature of the material, which dictates to either remove the heat of the melt as quickly as possible in order to avoid crystallization or to strongly limit the processing time for thermoplastic forming in the supercooled liquid region. Instead, the layer-wise construction of a component by local melting with a high-power laser (as in SLM) breaks down the cooling process into manifold steps, each of which is sufficiently fast to guarantee glass-formation – provided the proper alloy powder is employed. In the present work, glass-forming $Fe_{74}Mo_4P_{10}C_{7.5}B_{2.5}Si_2$ powder was used and it retains its amorphous structure after being processed in the SLM device under the appropriate conditions. Thus, it could be demonstrated that SLM is a suitable tool for producing amorphous metallic parts. The great advantage of selective laser melting is that in theory even marginal glass formers can be used and the dimensions and complexity of the final part is essentially limitless.

It should be mentioned here that the quality of the scaffold in the present work can be still improved by fine-tuning the processing parameters as well as the alloy composition. This will improve the surface finish, reduce the porosity and hamper the formation of cracks during solidification. Nevertheless, these first results underpin the feasibility of the current approach and disclose the potential of SLM as a technology to process metallic and bulk metallic glasses.

Acknowledgements

This research was funded by the European Union and the Free State of Saxony (13795/2379) in the framework of the European Centre for Emerging Materials and Processes (ECEMP). The authors are grateful to U. Wilke and B. Bartusch for help with the DSC measurements, L. Giebeler and P. Konda Gokuldoss for XRD measurements, H. Wendrock for SEM and S. Donath, M. Frey, H. Merker, and R. Taranczewski for technical assistance and stimulating discussions.

References

[1] C.A. Pampillo, J. Mater. Sci. 10 (1975) 1194–1227.
[2] A. Inoue, Acta Mater. 48 (2000) 279–306.
[3] A.L. Greer, Mater. Today 12 (2009) 14–22.
[4] D. Turnbull, Metall. Trans. B 12 (1981) 217–230.
[5] A.L. Greer, Science 267 (1995) 1947–1953.
[6] W.H. Wang, et al. Mater. Sci. Eng. R 44 (2004) 45–89.
[7] N. Nishiyama, et al. Intermetallics 30 (2012) 19–24.
[8] D. Turnbull, Cont. Phys. 10 (1969) 473–488.
[9] W.L. Johnson, Prog. Mater. Sci. 30 (1986) 81–134.
[10] A.L. Greer, E. Ma, MRS Bull. 32 (2007) 611–615.
[11] W.L. Johnson, MRS Bull. 24 (1999) 42–56.
[12] H.H. Liebermann, Mater. Sci. Eng. 43 (1980) 203–210.
[13] A. Inoue, A. Takeuchi, Acta Mater. 59 (2011) 2243–2267.
[14] W.H. Wang, et al. Appl. Phys. Lett. 74 (1999) 1803–1805.
[15] P. Chaudhari, D. Turnbull, Science 199 (1978) 11–21.
[16] D.B. Miracle, Nat. Mater. 3 (2004) 697–702.
[17] D.B. Miracle, et al. MRS Bull. 32 (2007) 629–634.
[18] M. Telford, Mater. Today 7 (2004) 36–43.
[19] M. Chen, Ann. Rev. Mater. Res. 38 (2008) 445–469.
[20] A. Inoue, et al. Nat. Mater. 2 (2003) 661–663.
[21] H.S. Chen, Rep. Prog. Phys. 43 (1980) 353–432.
[22] A.R. Yavari, et al. MRS Bull. 32 (2007) 635–638.
[23] C.A. Schuh, et al. Acta Mater. 55 (2007) 4067–4109.
[24] J.F. Löffler, Intermetallics 11 (2003) 529–540.
[25] C.A. Angell, Science 267 (1995) 1924–1935.
[26] J. Schroers, et al. Mater. Today 14 (2011) 14–19.
[27] N. Zhang, et al. Mater. Today 15 (2012) 216–221.
[28] J.P. Chu, et al. Appl. Phys. Lett. 90 (2007) 034101.
[29] A. Peker, W.L. Johnson, Appl. Phys. Lett. 63 (1993) 2342–2344.
[30] W.L. Johnson, et al. Science 332 (2011) 828–833.
[31] E.C. Santos, et al. Int. J. Mach. Tools Manuf. 46 (2006) 1459–1468.
[32] D.L. Bourell, et al. Int. J. Powder Metall. 28 (1992) 369–381.
[33] M.H. Elahinia, et al. Prog. Mater. Sci. 57 (2012) 911–946.
[34] B. Zheng, et al. Metall. Mater. Trans. A 40 (2009) 1235–1245.
[35] M. Rombouts, et al. CIRP Ann. – Manuf. Techn. 55 (2006) 187–192.
[36] P.S. Grant, Prog. Mater. Sci. 39 (1995) 497–545.
[37] F. Liu, et al. J. Alloys Compd. 483 (2009) 613–615.
[38] M. Stoica, et al. Phil. Mag. Lett. 86 (2006) 267–275.
[39] E.J. Lavernia, Y. Wu, Spray Atomization and Deposition, John Wiley and Sons, West Sussex, 1996, pp. 155–260.
[40] P. Dong, et al. J. Alloys Compd. 436 (2007) 118–123.